

Pseudospin Paramagnons and the Superconducting Dome in Magic Angle Twisted Bilayer Graphene

Chunli Huang, Nemin Wei, Wei Qin, and Allan H. MacDonald
Department of Physics, University of Texas at Austin, Austin TX 78712
 (Dated: October 27, 2021)

We present a theory of superconductivity in magic-angle twisted bilayer graphene in which attraction is generated between electrons on the same honeycomb sublattice when the system is close to a sublattice polarization instability. The resulting Cooper pairs are spin-polarized valley-singlets. Because the sublattice polarizability is mainly contributed by interband fluctuations, superconductivity occurs over a wide range of moiré filling fraction. It is suppressed by i) applying a sublattice polarizing field (generated by an aligned BN substrate) or ii) changing moiré band filling to favor valley polarization. The enhanced intrasublattice attraction close to sublattice polarization instability is analogous to enhanced like-spin attraction in liquid ^3He near the melting curve and the enhanced valley-singlet repulsion close to valley-polarization instabilities is analogous to enhanced spin-singlet repulsion in metals that are close to a ferromagnetic instability. We comment on the relationship between our pseudospin paramagnon model and the rich phenomenology of superconductivity in twisted bilayer and multilayer graphene.

Introduction:- Possible explanations for superconductivity in magic-angle twisted bilayer (trilayer) graphene MATB(T)G [1, 2] are increasingly constrained by experimental data [3–16]. The normal state properties revealed by the weak-field Hall effect and magnetoresistance oscillations [13] are particularly telling; the strongest superconductivity occurs within the moiré band filling interval $\nu \in (-3, -2)$, within which the system has a hole-like Fermi surfaces surrounding $|\nu|-2$ states per moiré period. The implied Fermi surface reconstruction points to symmetry breaking that depopulates two of four spin/valley flavors, an interpretation that is reinforced by Landau fans that are only doubly degenerate for $\nu \in (-3, -2)$ in spite of the systems four-fold spin/valley band degeneracy. The normal state symmetry breaking provides a natural explanation for large in-plane critical magnetic fields [14] that are $\sim 2-3$ times larger than the Clogston-Chandrasekhar limit of spin-singlet superconductors. As summarized in Fig. 1, superconductivity is suppressed as ν approaches -3 and as ν approaches -2 , filling factors at which the system is known to tend toward valley-ordered states, forming a dome in the system's (T, ν) phase diagram that is reminiscent of those observed in cuprate superconductors. For example, the superconducting critical temperature T_c of device 1 in Ref. [5] is peaked at $\nu \sim -2.4$, and vanishes near $\nu \rightarrow -2.7$ on the low-filling-factor side and near $\nu \rightarrow -2.2$ on the high filling factor side. The suppression of superconductivity on the low-filling factor side occurs in spite of an increasing Fermi level density-of-states, and therefore argues against a mechanism, like phonon-dressing, in which the pairing glue is external to the electron system. Superconductivity actually seems to be suppressed when the Fermi level is close to a the flat valence band van Hove singularity energy [2, 11]. These experimental observations point to an electronic pairing mechanism.

In this Letter, we argue that the superconducting

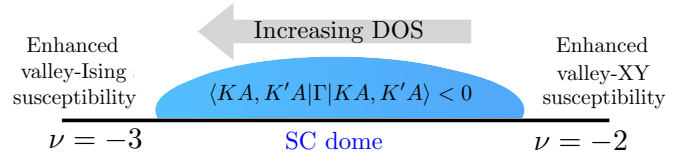


FIG. 1. Exchange-enhanced sublattice pseudospin polarizability leads to an attractive intrasublattice interaction that can support spin-triplet, valley-singlet superconductors across a wide range of moiré band filling fraction ν . Superconductivity is suppressed when ν is tuned close to valley polarization instabilities and when the density-of-states (DOS) is small.

properties of MATBG are consistent with a sublattice-pseudospin paramagnon pairing mechanism, and interpret the shape of the superconducting dome in terms of sublattice and valley paramagnons. Our main message is summarized in Fig. 1.

Pseudospin-paramagnons (PPM) and fermion pairing:- Our theory of MATBG superconductivity is guided by experiments [13, 14] and inspired by what is known about the relationship between fermion pairing in liquid ^3He and the strongly enhanced paramagnetic spin susceptibilities that appear near the solidification curve [20]. The enhanced susceptibility leads to a low-frequency neutral excitation spectrum that is dominated by *paramagon* peaks, damped collective modes that generate a strong attraction between like-spin nuclei, and leads to anisotropic spin-triplet Anderson-Brinkman-Morel [21] superfluidity. Spin-fluctuation mediated superfluidity in ^3He is succinctly captured by the paramagnon model, which uses a single exchange-interaction parameter I to describe the enhanced spin susceptibility [22]. The paramagnon model accounts quantitatively for the $T^3 \ln T$ contribution to heat capacity in ^3He [23], and has been extended to understand the interplay

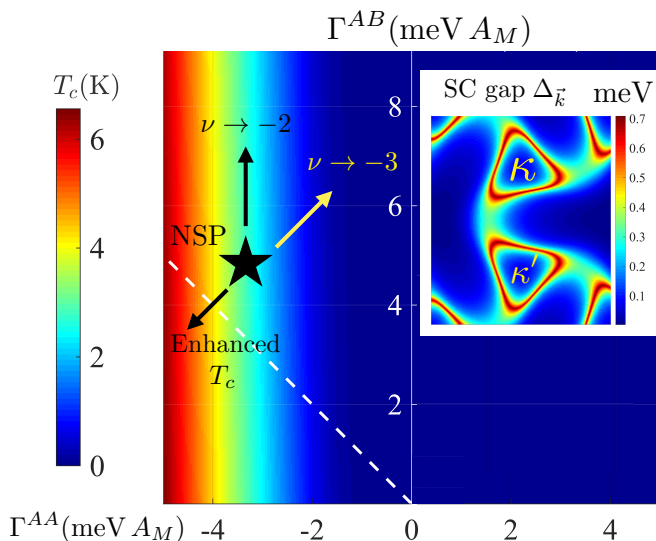


FIG. 2. T_c v.s. Γ^{AA} and Γ^{AB} . $A^a = (\Gamma^{AA} - \Gamma^{AB})/2$ is attractive and strong in nearly sublattice polarized (NSP) metals, whereas $A^s = (\Gamma^{AA} + \Gamma^{AB})/2$ is repulsive, but weak if screening is strong. Superconductivity occurs at low temperature when Γ^{AA} is attractive, even though Γ^{AB} is repulsive. The physically accessible parameter range above the dashed white $A^s = 0$ line includes superconductivity states. The inset plots the pairing self-energy $\Delta_{\mathbf{k}}$ vs. \mathbf{k} in the moiré Brillouin-zone for a continuum model with $t_{AA}/t_{AB} = 0.7$, at $\theta = 1.1^\circ$, at $\nu = -2.4$ [17]. $\Delta_{\mathbf{k}}$ is largest near the normal state Fermi surfaces centered on κ , κ' . When the system is close to a valley-Ising instability (near -3) or when it is sublattice polarized (near $\nu = +3$) [18, 19], $\nu = +1$ [11]), Γ^{AA} will increase and superconductivity will weaken. When A^s is decreased by the acoustic-phonon mediated interaction and/or screening of the long-range Coulomb interactions, T_c is enhanced. These trends are indicated by arrows and discussed in the main text.

between magnetism and superconductivity in metals, including heavy-fermion materials [24–26].

Unlike nuclei in ^3He , which possess only a spin degree of freedom, flat-band electrons in MATBG possess a spin(s) \times valley(τ) \times sublattice(σ) pseudospin octet that generates eight distinct states for each momentum and an abundance of potential pairing channels that has to be winnowed. Some progress can be achieved by taking note of the time-reversal symmetry property $\epsilon_{\mathbf{K}}(\mathbf{k}) = \epsilon_{\mathbf{K}'}(-\mathbf{k})$, which strongly favors Cooper pairing between electrons in opposite valleys \mathbf{K} and \mathbf{K}' ($\epsilon_{\mathbf{K}}(\mathbf{k}) \neq \epsilon_{\mathbf{K}}(-\mathbf{k})$). If we assume [13, 14] that the normal state for $\nu < -2$ is ferromagnetic (in spin), we can conclude that the Cooper pairs must be spin-polarized valley-singlets. That still leaves the sublattice pseudospin, and the need to overcome the strong sublattice independent Coulomb repulsion. A route to superconductivity is provided by the properties of the flatband spinors which imply, as illustrated in Fig. 2, that superconductivity occurs when the intrasublattice interaction is attractive ($\Gamma^{AA} < 0$) even if the intersublattice inter-

action is strongly repulsive ($\Gamma^{AB} > 0$) [27]. This property of magic-angle superconductivity is analogous to the robustness of spin-triplet superconductivity against repulsive opposite-spin interactions in systems with weak spin-orbit coupling [28], and can be traced to the D_6 point-group symmetry of the band Hamiltonian which decouples like-sublattice and unlike-sublattice pairing in the linearized gap equation [17]. We show below that intrasublattice attraction is generated when the system is close to a spontaneous sublattice polarization instability. This instability is common in graphene multilayers because sublattice polarization simplifies the spinor content of occupied states and increases exchange energies [29, 30]. The same analysis that shows that sublattice PPM bolster superconductivity, shows that valley PPM are obstructive.

Sublattice-Dependent Effective Interactions:-. The reduced pairing Hamiltonian for spin \uparrow electrons in opposite valleys is

$$H_{\text{red}} = \sum_{\mathbf{k}\mathbf{k}',\sigma_i} \left[\Gamma_{\mathbf{k}\mathbf{k}'}(\sigma_1\sigma_4; \sigma_2\sigma_3) \times c_{\mathbf{K}+\mathbf{k}'\sigma_1\uparrow}^\dagger c_{-\mathbf{K}-\mathbf{k}'\sigma_2\uparrow}^\dagger c_{-\mathbf{K}-\mathbf{k}\sigma_3\uparrow} c_{\mathbf{K}+\mathbf{k}\sigma_4\uparrow} \right], \quad (1)$$

where Γ is the particle-particle channel irreducible 4-point vertex function estimated below [31, 32], \mathbf{k} labels a state in the moiré valence band, and $\sigma = (A, B)$ labels sublattice. As we explain below, the PPM contributions to Γ are dominantly diagonal in sublattice at each vertex. This property motivates a model in which the dependence of Γ on \mathbf{k}, \mathbf{k}' is neglected and C_2 symmetry is recognized:

$$\Gamma_{\mathbf{k}\mathbf{k}'}(\sigma_1\sigma_4; \sigma_2\sigma_3) \rightarrow \delta_{\sigma_1,\sigma_4}\delta_{\sigma_2,\sigma_3} [\Gamma^{AA}\delta_{\sigma_1,\sigma_2} + \Gamma^{AB}\delta_{\sigma_1,-\sigma_2}]. \quad (2)$$

As illustrated in Fig. 2, superconductivity occurs in this model when the same sublattice effective interaction Γ^{AA} is attractive. The superconductivity gap is approximately uniform on the valley-projected FS (centered around κ and κ'), as shown in the inset. T_c is not suppressed by repulsive Γ^{AB} interactions because the susceptibility for pairs on opposite sublattices averages to zero on the Fermi surface. Motivated by this observation, we now address the relationship of Γ^{AA} to PPMs.

Recognizing that the computation of Γ from first-principles is a formidable challenge even in relatively simple systems [28, 33], we follow a phenomenological approach similar in spirit to that employed successfully in ^3He [24]. In that case spin-rotational invariance allows the spin-dependent effective interaction to be parameterized by just two scattering amplitudes, one each for the spin-symmetric and spin antisymmetric channel, (*i.e.* $\Gamma = A^s + A^a \mathbf{s}_1 \cdot \mathbf{s}_2$ [20]). In MATBG, the Hamiltonian is not invariant under rotations of the sublattice pseudospins. When the system is close to a sublattice-polarization instability, however, effective interactions

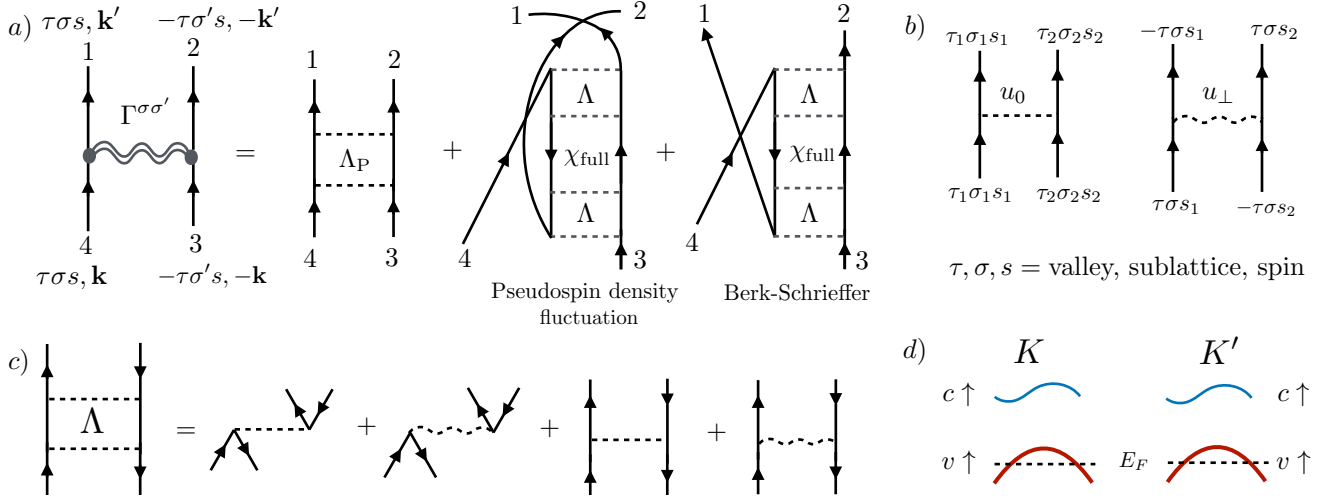


FIG. 3. a) The interaction potential Γ relevant to superconductivity has three contributions [31, 32]: a particle-particle vertex function Λ_P , a double-crossing diagram and the Berk-Schrieffer (single-crossing) diagram. The crossing diagrams relate Γ to paramagnon interactions that diverge at particle-hole instabilities. b) $u_0 > 0$ is a pseudospin-independent density-density interaction and $u_\perp > 0$ is an inter-valley scattering potential. c) The particle-hole vertex function Λ consists of the direct and exchange scattering terms from both u_0 and u_\perp . d) Schematic Fermi surface for $-3 < \nu < -2$ where $c(v)$ are the spin and valley projected conduction (valence) band.

that are diagonal in sublattice dominate and the analogous expressions are

$$\Gamma^{AA} = A^s + A^a, \quad \Gamma^{AB} = A^s - A^a. \quad (3)$$

We estimate A^s and A^a by assuming a simple δ -function interaction model in order to sum the Feynman diagrams specified by Fig. 3. The irreducible vertex function Λ accounts for both direct and exchange scattering (*i.e.* generalized-random-phase approximation) generated by u_0 and u_\perp . u_0 is the fully symmetric Coulomb interaction while the valley-exchange scattering term $u_\perp > 0$ breaks independent spin-rotation symmetry in opposite valleys and selects the spin-ferromagnet over other possibilities as the flavor-polarized normal state. [34]

Ignoring for the moment the Berk-Schrieffer transverse fluctuation diagram in Fig. 3, we find that

$$A^s = \frac{1}{2} (T^{\tau_0\sigma_0} - T^{\tau_z\sigma_0}), \quad A^a = \frac{1}{2} (T^{\tau_0\sigma_z} - T^{\tau_z\sigma_z}), \quad (4)$$

where

$$T^{\tau_0\sigma_0} = \frac{1}{2} \frac{3u_0 - u_\perp}{1 + (3u_0 - u_\perp)\chi_{\mathbf{k}-\mathbf{k}',\omega}^{K\sigma_0,K\sigma_0}}, \quad (5)$$

$$T^{\tau_z\sigma_0} = -\frac{1}{2} \frac{u_0 - u_\perp}{1 - (u_0 - u_\perp)\chi_{\mathbf{k}-\mathbf{k}',\omega}^{K\sigma_0,K\sigma_0}}, \quad (6)$$

$$T^{\tau_0\sigma_z} = -\frac{1}{2} \frac{u_0 + u_\perp}{1 - (u_0 + u_\perp)\chi_{\mathbf{k}-\mathbf{k}',\omega}^{K\sigma_z,K\sigma_z}}, \quad (7)$$

$$T^{\tau_z\sigma_z} = -\frac{1}{2} \frac{u_0 - u_\perp}{1 - (u_0 - u_\perp)\chi_{\mathbf{k}-\mathbf{k}',\omega}^{K\sigma_z,K\sigma_z}}, \quad (8)$$

Here $\chi_{\mathbf{q},\omega=0}^{O,O^\dagger}$ is a bare susceptibility for pseudospin polarization O . We discuss the valley-diagonal, sublattice even ($\chi_{\mathbf{q},\omega=0}^{K\sigma_0,K\sigma_0}$) and sublattice odd ($\chi_{\mathbf{q},\omega=0}^{K\sigma_z,K\sigma_z}$) susceptibilities further below.

The random phase sums decouple contributions that are proportional to different products of valley and sublattice Pauli matrices (τ_0 or τ_z and σ_0 or σ_z) of the interacting particle-hole pairs and yield pseudospin-dependent interactions that are sums of the four different geometric series. In each of the $T^{\tau_a\sigma_b}$'s a bare interaction is modified by a dressing factor (*i.e.* denominator) identical to the one that modifies the corresponding susceptibility. For the valley and sublattice independent interaction $T^{\tau_0\sigma_0}$ the bare interaction is dominated by the bare repulsive Coulomb interaction u_0 and the modification is suppression due to static screening. For all other interaction channels, the dominant bare contribution is an attractive exchange contribution and the modification factor yields enhancement. At lowest order $\Gamma^{AA} = u_0 - u_\perp$ and $\Gamma^{AB} = u_0$ are both repulsive. Superconductivity is possible when $T^{\tau_0\sigma_z}$, which contributes attractively to Γ^{AA} , has much larger enhancement factors than $T^{\tau_z\sigma_0}$ and $T^{\tau_z\sigma_z}$, both of which contribute repulsively and diverge at valley polarization instabilities. We conclude that attractive intra-sublattice effective interactions, and hence superconductivity, is likely when the system is close to a valley-independent sublattice polarization instability but far from a valley-polarization instabilities.

We have so far neglected the Berk-Schrieffer (BS) transverse valley fluctuations indicated in Fig. 3. The particle-hole channels in the BS diagrams decouple into four channels $\tau_+\sigma_{0,x,y,z}$ in the long wavelength limit.

They change

$$A^{s,a} \rightarrow A^{s,a} \mp \frac{1}{2} \sum_{i=x,y} T^{\tau+\sigma_i} - \frac{1}{2} \sum_{\delta=0,z} T^{\tau+\sigma_\delta}. \quad (9)$$

Because the susceptibilities in the $\delta = 0, z$ channels excite particle-hole pair from opposite Chern bands, their average transition matrix elements are small [35, 36]. As shown in Ref. [17], they are in fact smaller than the susceptibility in the pseudospin density fluctuation channels. The other two channels in the BS diagrams ($i = x, y$) are off-diagonal in sublattice and therefore do not affect the attractive interaction Γ^{AA} . As a result, the net effect of transverse valley fluctuations (which can be strong close to intervalley coherent order [37–39]) is to increase Γ^{AB} in the vertical direction shown in Fig. 2 and do not modify the T_c . Hence, transverse valley fluctuations can be neglected in our analysis. In making these estimates of importance, we are not considering the possibility of a nodal superconducting gap generated by repulsive interactions with strong momentum dependence - something that cannot be ruled out.

In the analysis of spin-fluctuation mediated Cooper pairing in liquid ^3He and other Fermi-systems with weak spin-orbit coupling, there is often no need to distinguish the longitudinal spin-fluctuation double-crossing diagram from the transverse spin-fluctuation Berk-Schrieffer diagram because the pairing interaction is invariant under $\text{SU}(2)$ spin rotation. This distinction is important in our present analysis because the pseudospin ($\tau \otimes \sigma$) anisotropic energy arose from the band Hamiltonian is very large and as a result, the transverse and longitudinal pseudospin fluctuations can contribute independently to the pairing interaction.

The Superconducting Dome:-. We are now in a position to explain how the distinct filling factor dependencies of the different $T^{\tau_a\sigma_b}$'s forms the superconducting dome. An enhanced sublattice polarization susceptibility, which strengthens an attractive interaction, is present when the corresponding Stoner criterion $(u_0 + u_\perp)\chi_{\mathbf{q},\omega=0}^{K\sigma_z,K\sigma_z} = 1$, is nearly satisfied. Repulsive interactions are strengthened when one of the valley polarization susceptibilities, with Stoner criteria $(u_0 - u_\perp)\chi_{\mathbf{q},\omega=0}^{K\sigma_0,K\sigma_0} = 1$ or $(u_0 - u_\perp)\chi_{\mathbf{q},\omega=0}^{K\sigma_z,K\sigma_z} = 1$, are close to being satisfied. Because $u_0 + u_\perp$ is larger than $u_0 - u_\perp$ the attractive $\tau_0\sigma_z$ channel interaction is always stronger than the repulsive $\tau_z\sigma_z$ channel. Physically, the $\tau_0\sigma_z$ susceptibility is enhanced and the $\tau_z\sigma_z$ susceptibility suppressed by u_\perp because its exchange energy is maximized when opposite valleys have identical sublattice polarization. The competition between normal and superconducting states is therefore between the sublattice polarization Stoner criteria, which involves the $\chi_{\mathbf{q},\omega=0}^{K\sigma_z,K\sigma_z}$ polarization, and the valley polarization Stoner criterion, which involves $\chi_{\mathbf{q},\omega=0}^{K\sigma_0,K\sigma_0}$. Because of \mathcal{C}_2T symmetry (where T is a spinless time-reversal symmetry) these two polarizations have

very distinct dependencies on band filling. In particular $\chi_{\mathbf{q}\rightarrow 0,\omega=0}^{K\sigma_z,K\sigma_z}$ does not have an intraband contributions because the expectation value of σ_z is zero in all moiré band states. Its value is therefore not related to peaks in the band density-of-states and, as illustrated in Fig. 3d, should instead be larger closer to $\nu = -2$ where the majority spins are nearly half-filled and the interband transition phase space is therefore largest. On the other hand, $\chi_{\mathbf{q}\rightarrow 0,\omega=0}^{K\sigma_0,K\sigma_0}$ is proportional to the Fermi level density of states and increases rapidly as $|\nu| - 2$ increases and the Fermi level approaches the Van Hove peak in the valence moiré band. We attribute the suppression of superconductivity on the large $|\nu| - 2$ side of the superconducting dome to the increasingly strong repulsive interaction contribution to A^s from $T^{\tau_z\sigma_0}$, which is proportional to the valley polarization susceptibility enhancement factor and suppresses superconductivity, as indicated in Fig. 2. On the other hand, we attribute the suppression of superconductivity on the small $|\nu| - 2$ side of the dome to the decreasing Fermi-level density-of-states.

We emphasize that our picture of superconductivity in graphene moiré superlattice requires that the normal state is nearly sublattice polarized metal over a wide range of filling fraction. Enhanced sublattice polarization, and sometimes sublattice polarization instabilities, are in fact common in all graphene multilayer electron gas systems [29]. For example, neutral Bernal bilayer graphene has $\sigma_z s_z$ order, *i.e.* spin-dependent sublattice-polarization in the antiferromagnetic state [30]. In twisted bilayers the gaps between flat and remote bands open an opportunity for flavor polarization and hence for sublattice polarization not only near neutrality but also near integer ν . In moiré flat bands itinerant exchange energies favor maximum spin-polarization before orbital-polarization, allowing the majority spin projected conduction and valence bands to mix and produce finite sublattice polarization over a wide range of filling fraction.

Summary and Discussions:- Paramagnon-mediated pairing physics in MATBG is enriched by the relevance of spin, valley, and sublattice pseudospins. Because the valley-projected bands are not time-reversal invariant, pairing is likely to occur between time-reversal partner states in opposite valleys and yield valley-singlets. We have shown that valley-singlet superconductivity occurs in MATBG when the effective interaction between electrons on the same sublattice is attractive, and that this condition is satisfied when the system is close to a sublattice-polarization instability, but far from a valley-polarization instability. There is no need for the interaction between electrons on opposite sublattice, or the total interaction summed over sublattices, to be attractive. Enhanced intrasublattice attraction close to sublattice polarization instabilities is analogous to the enhanced like-spin attraction in ^3He [21] near the melting curve, and enhanced valley-singlet repulsion close to

valley-polarization instabilities is analogous to enhanced spin-singlet repulsion [22] in metals that are close to a ferromagnetic instability. Together these two effects explain the prominent superconducting domes seen in most MATBG samples inside the filling factor interval $\nu \in (2, 3)$ [40].

We now comment on other aspects of the phenomenology of MATBG superconductivity seen through the pseudospin paramagnon lens:

i) *Influence of Boron-Nitride (hBN) Alignment*:– Aligned hBN induces a finite sublattice polarization in a graphene sheet, and weakens sublattice pseudospin fluctuations. Since all other contributions to the intrasublattice interaction are repulsive, this theory predicts that superconductivity is suppressed by hBN alignment, in agreement with current experimental findings.

ii) *Coulomb screening*:– When MATBG devices are surrounded by nearby material that is conducting [5, 9, 41] or has a large dielectric constant [42], insulating states at integer filling factors become less prominent in the phase diagram and superconductivity is found over a broader range of filling factors. Insulating states are understood in terms of exchange-splitting between bands associated with different flavor states that is larger than the flatband bandwidth. Since the exchange splittings are dominated by the Coulomb interaction u_0 , they are expected to be reduced by enhanced environmental screening. The reduction in insulating state gaps seen experimentally is therefore expected. On the other hand, the net attractive interaction contributed by $T^{\tau_0\sigma_z} - T^{\tau_z\sigma_z}$ scales with the intervalley-exchange interaction u_\perp , which should not be influenced by environmental screening. In addition the enhancement factors in $T^{\tau_0\sigma_z}$ and $T^{\tau_z\sigma_z}$, which together contribute attractively to Γ^{AA} , both involve the $\chi_{\mathbf{q},\omega}^{K\sigma_z,K\sigma_z}$ susceptibility which does not have a $\mathbf{q} = 0$ Fermi surface contribution. $\chi_{\mathbf{q},\omega}^{K\sigma_z,K\sigma_z}$ is instead dominated by interband fluctuations that are less sensitive to remote screening. On the other hand, $T^{\tau_0\sigma_0}$, the repulsive screened Coulomb interaction, is certainly weakened by enhanced dielectric screening. The net result of enhanced remote screening could therefore be to enhance superconductivity, as sometimes observed experimentally. Although both superconductivity and insulating behavior require interactions, remote screening influences only u_0 , and can therefore have opposite influences on the two states.

iii) *Superconductivity near $\nu = 0$* :– Although superconductivity is most robustly observed for $\nu \in (2, 3)$, the hole-like and electron-like Fermi surfaces on opposite side of $\nu = 0$ also sometimes host superconductivity as shown in Ref. [4]. Since our proposed theory of superconductivity between $-3 < \nu < -2$ only involves states in a spin-projected Hilbert space (*c.f.* Fig. 3d), it can be extended to $-1 < \nu < +1$ by assuming an identical pairing mechanism occurs in in both spin projected Hilbert spaces. This state would be similar to

the equal spin pairing state in ^3He . The stronger superconductivity for $-3 < \nu < -2$, could be attributed to band-renormalizations that flatten bands away from half-filling. [15, 43–45].

iv) *Particle-hole asymmetry of superconductivity*:– Experiment shows that the tendency toward valley polarization, which opposes superconductivity, is stronger for electron-doped than for hole-doped MATBG. This tendency is due in part to conduction bands that are less dispersive than the valence bands, and have a different shape [15, 43–45]. It is quite likely that the normal state on the electron-doped side is a sublattice ferromagnet, as is supported by the observation of the anomalous Hall effect over a wide range of filling factors near $\nu = 3$ in devices with aligned hBN [18, 19] and in $\nu = 1$ [11] without aligned hBN. In addition, the valley PPMs that suppress superconductivity are certain to be stronger on the electron-doped side.

v) *Phonon mediated pairing* [46–51]:– Optical (acoustic) phonon mediated interactions are outside (inside) the interaction parameter space spanned by Γ^{AA} and Γ^{AB} . Explicit gap equation solutions [47, 48] show that optical phonons can induce superconductivity if the repulsive Coulomb interaction is somehow strongly suppressed. When the acoustic phonon propagator is not screened by electrons, it leads to a ν -independent attraction $\Gamma^{AA} = A^s \sim -0.5\text{meV}$ [48] that is too small to explain the superconductivity dome. As shown in Fig. 2, since acoustic phonons reduce A_s [52], they can nevertheless play a role in enhancing T_c .

The pseudospin paramagnon is able to account for many aspects of the rich phenomenology of MATBG, including the mismatch between conditions that favor superconductivity and the anomalous Hall effect, the influence of enhanced remote screening, and particle-hole asymmetry. Our proposal can be tested by systematically studying how encapsulating hBN alignment and remote screening influence superconductivity. It is interesting to contrast superconductivity in MATBG with the recently discovered [53] superconductivity in ABC trilayer graphene, which also has spin, valley, and sublattice pseudospins and has the advantage of simpler underlying electronic structure. In both cases, pairing is likely to occur between electrons in opposite valleys because the valley-projected bands are not time-reversal invariant. In ABC trilayers superconductivity appears to be enhanced by proximity to a transition that occurs between unbroken-symmetry and partially flavor polarized states. The difference between the two cases may lie in the underlying physics that controls sublattice polarization instabilities.

Acknowledgement:– We acknowledge informative conversations with Youngjoon Choi, Andrea Young and Haoxin Zhou. This work was supported by the U.S. Department of Energy, Office of Science, Basic Energy Sciences, under Award DE-SC0022106.

-
- [1] Y. Cao, V. Fatemi, S. Fang, K. Watanabe, T. Taniguchi, E. Kaxiras, and P. Jarillo-Herrero, “Unconventional superconductivity in magic-angle graphene superlattices,” *Nature*, vol. 556, no. 7699, pp. 43–50, 2018.
- [2] J. M. Park, Y. Cao, K. Watanabe, T. Taniguchi, and P. Jarillo-Herrero, “Tunable strongly coupled superconductivity in magic-angle twisted trilayer graphene,” *Nature*, vol. 590, no. 7845, pp. 249–255, 2021.
- [3] M. Yankowitz, S. Chen, H. Polshyn, Y. Zhang, K. Watanabe, T. Taniguchi, D. Graf, A. F. Young, and C. R. Dean, “Tuning superconductivity in twisted bilayer graphene,” *Science*, vol. 363, no. 6431, pp. 1059–1064, 2019.
- [4] X. Lu, P. Stepanov, W. Yang, M. Xie, M. A. Aamir, I. Das, C. Urgell, K. Watanabe, T. Taniguchi, G. Zhang, *et al.*, “Superconductors, orbital magnets and correlated states in magic-angle bilayer graphene,” *Nature*, vol. 574, no. 7780, pp. 653–657, 2019.
- [5] Y. Saito, J. Ge, K. Watanabe, T. Taniguchi, and A. F. Young, “Independent superconductors and correlated insulators in twisted bilayer graphene,” *Nature Physics*, vol. 16, no. 9, pp. 926–930, 2020.
- [6] H. Polshyn, M. Yankowitz, S. Chen, Y. Zhang, K. Watanabe, T. Taniguchi, C. R. Dean, and A. F. Young, “Large linear-in-temperature resistivity in twisted bilayer graphene,” *Nature Physics*, vol. 15, no. 10, pp. 1011–1016, 2019.
- [7] Y. Cao, D. Chowdhury, D. Rodan-Legrain, O. Rubies-Bigorda, K. Watanabe, T. Taniguchi, T. Senthil, and P. Jarillo-Herrero, “Strange metal in magic-angle graphene with near planckian dissipation,” *Physical review letters*, vol. 124, no. 7, p. 076801, 2020.
- [8] F. K. de Vries, E. Portolés, G. Zheng, T. Taniguchi, K. Watanabe, T. Ihn, K. Ensslin, and P. Rickhaus, “Gate-defined josephson junctions in magic-angle twisted bilayer graphene,” *Nature Nanotechnology*, pp. 1–4, 2021.
- [9] X. Liu, Z. Wang, K. Watanabe, T. Taniguchi, O. Vafek, and J. Li, “Tuning electron correlation in magic-angle twisted bilayer graphene using coulomb screening,” *Science*, vol. 371, no. 6535, pp. 1261–1265, 2021.
- [10] D. Wong, K. P. Nuckolls, M. Oh, B. Lian, Y. Xie, S. Jeon, K. Watanabe, T. Taniguchi, B. A. Bernevig, and A. Yazdani, “Cascade of electronic transitions in magic-angle twisted bilayer graphene,” *Nature*, vol. 582, no. 7811, pp. 198–202, 2020.
- [11] P. Stepanov, M. Xie, T. Taniguchi, K. Watanabe, X. Lu, A. H. MacDonald, B. A. Bernevig, and D. K. Efetov, “Competing zero-field chern insulators in superconducting twisted bilayer graphene,” *arXiv preprint arXiv:2012.15126*, 2020.
- [12] U. Zondiner, A. Rozen, D. Rodan-Legrain, Y. Cao, R. Queiroz, T. Taniguchi, K. Watanabe, Y. Oreg, F. von Oppen, A. Stern, *et al.*, “Cascade of phase transitions and dirac revivals in magic-angle graphene,” *Nature*, vol. 582, no. 7811, pp. 203–208, 2020.
- [13] Y. Saito, F. Yang, J. Ge, X. Liu, T. Taniguchi, K. Watanabe, J. Li, E. Berg, and A. F. Young, “Isospin pomeranchuk effect in twisted bilayer graphene,” *Nature*, vol. 592, no. 7853, pp. 220–224, 2021.
- [14] Y. Cao, J. M. Park, K. Watanabe, T. Taniguchi, and P. Jarillo-Herrero, “Pauli-limit violation and re-entrant superconductivity in moiré graphene,” *Nature*, vol. 595, no. 7868, pp. 526–531, 2021.
- [15] Y. Choi, H. Kim, C. Lewandowski, Y. Peng, A. Thomson, R. Polski, Y. Zhang, K. Watanabe, T. Taniguchi, J. Alicea, *et al.*, “Interaction-driven band flattening and correlated phases in twisted bilayer graphene,” *arXiv preprint arXiv:2102.02209*, 2021.
- [16] Y. Choi, H. Kim, Y. Peng, A. Thomson, C. Lewandowski, R. Polski, Y. Zhang, H. S. Arora, K. Watanabe, T. Taniguchi, *et al.*, “Correlation-driven topological phases in magic-angle twisted bilayer graphene,” *Nature*, vol. 589, no. 7843, pp. 536–541, 2021.
- [17] Supplementary-materials
- [18] M. Serlin, C. Tschirhart, H. Polshyn, Y. Zhang, J. Zhu, K. Watanabe, T. Taniguchi, L. Balents, and A. Young, “Intrinsic quantized anomalous hall effect in a moiré heterostructure,” *Science*, vol. 367, no. 6480, pp. 900–903, 2020.
- [19] A. L. Sharpe, E. J. Fox, A. W. Barnard, J. Finney, K. Watanabe, T. Taniguchi, M. Kastner, and D. Goldhaber-Gordon, “Emergent ferromagnetism near three-quarters filling in twisted bilayer graphene,” *Science*, vol. 365, no. 6453, pp. 605–608, 2019.
- [20] K. Levin and O. T. Valls, “Phenomenological theories of liquid 3He ,” *Physics Reports*, vol. 98, no. 1, pp. 1–56, 1983.
- [21] P. W. Anderson and W. Brinkman, “Anisotropic superfluidity in He^3 : A possible interpretation of its stability as a spin-fluctuation effect,” *Physical Review Letters*, vol. 30, no. 22, p. 1108, 1973.
- [22] N. Berk and J. Schrieffer, “Effect of ferromagnetic spin correlations on superconductivity,” *Physical Review Letters*, vol. 17, no. 8, p. 433, 1966.
- [23] S. Doniach and S. Engelsberg, “Low-temperature properties of nearly ferromagnetic fermi liquids,” *Physical Review Letters*, vol. 17, no. 14, p. 750, 1966.
- [24] P. W. Anderson, “Heavy-electron superconductors, spin fluctuations, and triplet pairing,” *Phys. Rev. B*, vol. 30, pp. 1549–1550, Aug 1984.
- [25] T. Moriya, “Developments of the theory of spin fluctuations and spin fluctuation-induced superconductivity,” *Proceedings of the Japan Academy, Series B*, vol. 82, no. 1, pp. 1–16, 2006.
- [26] D. J. Scalapino, “A common thread: The pairing interaction for unconventional superconductors,” *Rev. Mod. Phys.*, vol. 84, pp. 1383–1417, Oct 2012.
- [27] It is also true that attractive intersublattice interactions $\Gamma^{AB} < 0$ produce superconductivity when the intrasublattice interaction is repulsive. See [17] for a discussion of this case.
- [28] P. Anderson and W. Brinkman, “Theory of anisotropic superfluidity in He^3 ,” in *Basic Notions of Condensed Matter Physics*, pp. 287–388, CRC Press, 2018.
- [29] A. H. MacDonald, J. Jung, and F. Zhang, “Pseudospin order in monolayer, bilayer and double-layer graphene,” *Physica Scripta*, vol. 2012, no. T146, p. 014012, 2012.
- [30] J. Velasco, L. Jing, W. Bao, Y. Lee, P. Kratz, V. Aji, M. Bockrath, C. Lau, C. Varma, R. Stillwell, *et al.*, “Transport spectroscopy of symmetry-broken insulating states in bilayer graphene,” *Nature nanotechnology*, vol. 7, no. 3, pp. 156–160, 2012.
- [31] G. Vignale and K. Singwi, “Effective two-body interaction in coulomb fermi liquids,” *Physical Review B*, vol. 32, no. 4, p. 2156, 1985.
- [32] N. Bickers, “Self-consistent many-body theory for con-

- densed matter systems,” in *Theoretical Methods for Strongly Correlated Electrons*, pp. 237–296, Springer, 2004.
- [33] M. Nava, A. Motta, D. Galli, E. Vitali, and S. Moroni, “Equation of state of two-dimensional 3 he at zero temperature,” *Physical Review B*, vol. 85, no. 18, p. 184401, 2012.
- [34] We use crossing-symmetry [32] to relate the vertex functions in the particle-particle channel (Λ_P) to the one in particle-hole channel (Λ).
- [35] N. Bultinck, E. Khalaf, S. Liu, S. Chatterjee, A. Vishwanath, and M. P. Zaletel, “Ground state and hidden symmetry of magic-angle graphene at even integer filling,” *Physical Review X*, vol. 10, no. 3, p. 031034, 2020.
- [36] B. Lian, Z.-D. Song, N. Regnault, D. K. Efetov, A. Yazdani, and B. A. Bernevig, “Twisted bilayer graphene. iv. exact insulator ground states and phase diagram,” *Phys. Rev. B*, vol. 103, p. 205414, May 2021.
- [37] N. Bultinck, S. Chatterjee, and M. P. Zaletel, “Mechanism for anomalous hall ferromagnetism in twisted bilayer graphene,” *Physical Review Letters*, vol. 124, no. 16, p. 166601, 2020.
- [38] Y.-H. Zhang, D. Mao, Y. Cao, P. Jarillo-Herrero, and T. Senthil, “Nearly flat chern bands in moiré superlattices,” *Physical Review B*, vol. 99, no. 7, p. 075127, 2019.
- [39] J. Y. Lee, E. Khalaf, S. Liu, X. Liu, Z. Hao, P. Kim, and A. Vishwanath, “Theory of correlated insulating behaviour and spin-triplet superconductivity in twisted double bilayer graphene,” *Nature communications*, vol. 10, no. 1, pp. 1–10, 2019.
- [40] When the filling factor ν approaches $\nu = -3$, the enhanced valley polarizability not only generates a valley-singlet repulsion but also an attraction between electrons in the same valley. When this attraction leads to condensation of Cooper pairs from the same valley, the resulting superconducting order parameter cannot be uniform-s-wave because of Fermi statistics. (We assume the normal state is always spin-polarized). This means the order parameter might undergo a transition from valley-singlet to valley-triplet as $\nu \rightarrow -3$ and might explain the $U - V$ transition recently observed in local-tunneling spectroscopy [?]. In this scenario, valley-triplet superconductivity close to $\nu = -3$ is eventually suppressed by the enhanced pair-breaking (trigonal-warping) potential from the band-Hamiltonian.
- [41] P. Stepanov, I. Das, X. Lu, A. Fahimniya, K. Watanabe, T. Taniguchi, F. H. Koppens, J. Lischner, L. Levitov, and D. K. Efetov, “Untying the insulating and superconducting orders in magic-angle graphene,” *Nature*, vol. 583, no. 7816, pp. 375–378, 2020.
- [42] H. S. Arora, R. Polski, Y. Zhang, A. Thomson, Y. Choi, H. Kim, Z. Lin, I. Z. Wilson, X. Xu, J.-H. Chu, *et al.*, “Superconductivity in metallic twisted bilayer graphene stabilized by wse 2,” *Nature*, vol. 583, no. 7816, pp. 379–384, 2020.
- [43] T. Cea, N. R. Walet, and F. Guinea, “Electronic band structure and pinning of fermi energy to van hove singularities in twisted bilayer graphene: A self-consistent approach,” *Phys. Rev. B*, vol. 100, p. 205113, Nov 2019.
- [44] F. Guinea and N. R. Walet, “Electrostatic effects, band distortions, and superconductivity in twisted graphene bilayers,” *Proceedings of the National Academy of Sciences*, vol. 115, no. 52, pp. 13174–13179, 2018.
- [45] M. Xie and A. H. MacDonald, “Weak-field hall resistivity and spin/valley flavor symmetry breaking in matbg,” *arXiv preprint arXiv:2010.07928*, 2020.
- [46] Y. W. Choi and H. J. Choi, “Strong electron-phonon coupling, electron-hole asymmetry, and nonadiabaticity in magic-angle twisted bilayer graphene,” *Physical Review B*, vol. 98, no. 24, p. 241412, 2018.
- [47] F. Wu, A. MacDonald, and I. Martin, “Theory of phonon-mediated superconductivity in twisted bilayer graphene,” *Physical review letters*, vol. 121, no. 25, p. 257001, 2018.
- [48] W. Qin, B. Zou, and A. H. MacDonald, “Critical magnetic fields and electron-pairing in magic-angle twisted bilayer graphene,” *arXiv preprint arXiv:2102.10504*, 2021.
- [49] D. Abanin and L. Levitov, “Quantized transport in graphene pn junctions in a magnetic field,” *Science*, vol. 317, no. 5838, pp. 641–643, 2007.
- [50] E. Codecido, Q. Wang, R. Koester, S. Che, H. Tian, R. Lv, S. Tran, K. Watanabe, T. Taniguchi, F. Zhang, *et al.*, “Correlated insulating and superconducting states in twisted bilayer graphene below the magic angle,” *Science advances*, vol. 5, no. 9, p. eaaw9770, 2019.
- [51] R. Ojajärvi, T. Hyart, M. A. Silaev, and T. T. Heikkilä, “Competition of electron-phonon mediated superconductivity and stoner magnetism on a flat band,” *Physical Review B*, vol. 98, no. 5, p. 054515, 2018.
- [52] T. Cea and F. Guinea, “Coulomb interaction, phonons, and superconductivity in twisted bilayer graphene,” *Proceedings of the National Academy of Sciences*, vol. 118, no. 32, 2021.
- [53] H. Zhou, T. Xie, T. Taniguchi, K. Watanabe, and A. F. Young, “Superconductivity in rhombohedral trilayer graphene,” *arXiv preprint arXiv:2106.07640*, 2021.
- [54] W. Qin and A. H. MacDonald, “In-plane critical magnetic fields in magic-angle twisted trilayer graphene,” 2021.
- [55] D. Scalapino, “Superconductivity and spin fluctuations,” *Journal of Low Temperature Physics*, vol. 117, no. 3, pp. 179–188, 1999.

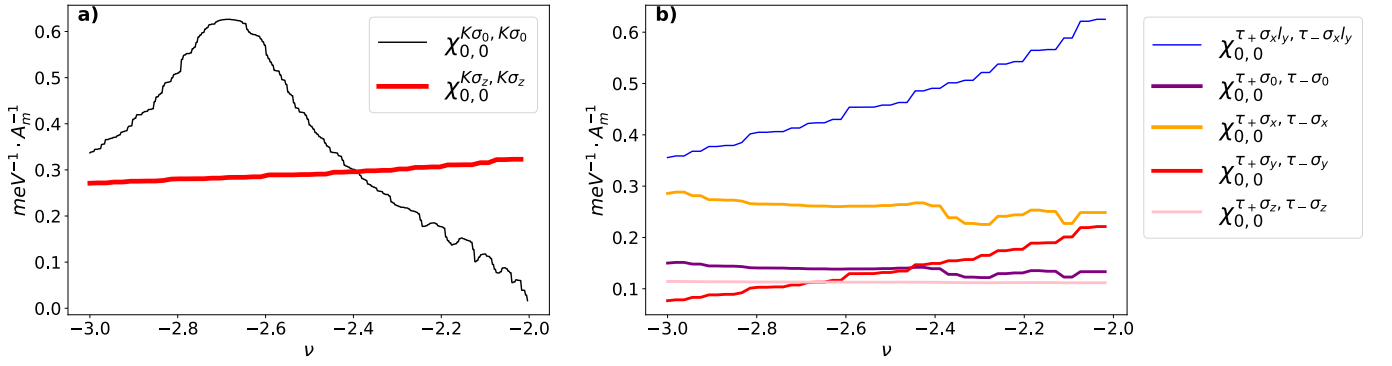


FIG. S1. The static uniform susceptibilities of twisted bilayer graphene in a) pseudospin density channels b) transverse valley channels. τ, σ, l represent valley, sublattice and layer degrees of freedom, respectively.

Supplementary Material: Pseudospin Paramagnons and the Superconducting Dome in Magic Angle Twisted Bilayer Graphene

I. NON-INTERACTING SUSCEPTIBILITIES IN VARIOUS PSEUDOSPIN CHANNELS

In the main text, we explain the superconducting dome in magic angle twisted bilayer graphene (MATBG) by considering a sublattice-dependent interaction potential that depends sensitively on the moiré band filling factor ν . We focus on $-2 < \nu < -3$. We show that MATBG is at the border of sublattice polarization over a wide range of ν and this generates an attractive intra-sublattice interaction between spin-polarized charge carriers in opposite valley and leads to superconductivity. This superconducting channel is suppressed as $\nu \rightarrow -3$ because the valley polarizability increases and as $\nu \rightarrow -2$ because the density of states at the Fermi level diminish.

In this section, we use a simple bandstructure model to calculate the non-interacting susceptibilities in various pseudospin channels to support our explanation to the superconducting dome. The bandstructure is obtained from the Bistritzer-MacDonald continuum model at twist angle $\theta = 1.15^\circ$ parametrized by interlayer tunneling parameters $t_{AB} = 110\text{meV}$ and $t_{AA} = 77\text{meV}$ for AB and AA bilayer stacking, respectively. We also include a nonlocal momentum-dependent correction to the interlayer tunneling, $dt_{AA}/dk = dt_{AB}/dk = -0.1$ [54]. Because there is no consensus on the Fermiology in MATBG (e.g. the location of the Fermi-surface after reset transition at $\nu = -2$), we will only make conclusions that are not sensitive to the details of the bandstructure.

As discussed in the main text, the normal state is spin-polarized so we consider only particle-hole excitations in the majority-spin projected Hilbert space. The pseudospin susceptibility of a particle-hole channel \mathcal{O} is defined as follows:

$$\chi_{\mathbf{q}, \omega}^{\mathcal{O}, \mathcal{O}^\dagger} = -i \int_0^\infty dt e^{i\omega t} \left\langle \frac{1}{A} \left[\sum_{\mathbf{p}, \alpha\beta} c_{\mathbf{p}, \alpha}^\dagger \mathcal{O}_{\alpha\beta} c_{\mathbf{p}+\mathbf{q}, \beta}, \sum_{\mathbf{p}', \alpha'\beta'} c_{\mathbf{p}'+\mathbf{q}, \alpha'}^\dagger \mathcal{O}_{\alpha'\beta'}^\dagger c_{\mathbf{p}', \beta'} \right] \right\rangle \quad (\text{S1})$$

$$= \frac{1}{A} \sum_{\mathbf{k} \in \text{B.Z.}, \tau m, \tau' n} \frac{n_F(\epsilon_{\tau m \mathbf{k} + \mathbf{q}}) - n_F(\epsilon_{\tau' n \mathbf{k}})}{\omega + \epsilon_{\tau' n \mathbf{k}} - \epsilon_{\tau m \mathbf{k} + \mathbf{q}} + i\delta} |\mathcal{M}_{\tau' n \mathbf{k}, \tau m \mathbf{k} + \mathbf{q}}|^2 \quad (\text{S2})$$

$$\mathcal{M}_{\tau' n \mathbf{k}, \tau m \mathbf{k} + \mathbf{q}} = \sum_{\mathbf{G}, \alpha\beta} \psi_{n\alpha}^*(\mathbf{k} + \mathbf{G}) \mathcal{O}_{\alpha\beta} \psi_{m\beta}(\mathbf{k} + \mathbf{q} + \mathbf{G}), \quad \alpha = \tau' \sigma' l' (\beta = \tau \sigma l) \quad (\text{S3})$$

Here α, β labels sublattice σ , valley τ and layer l degree of freedoms. In Eq. (S2), the basis is transformed from the plane-wave basis to the single-particle band basis. $|\tau n \mathbf{k}\rangle = \sum_{\mathbf{G}\sigma l} \psi_{n\tau\sigma l}(\mathbf{k} + \mathbf{G}) |\tau \sigma l, \mathbf{k} + \mathbf{G}\rangle$ is a state in band n with energy $\epsilon_{n\mathbf{k}}$, where \mathbf{k} is restricted to the first Brillouin zone (chosen to be centered around the Moiré m point) and the Bloch wave functions in two valleys are related by $\psi_{n+\sigma l}(\mathbf{k} + \mathbf{G}) = \psi_{n-\sigma l}^*(-\mathbf{k} - \mathbf{G})$. n_F is the Fermi-Dirac distribution and we set temperature $T = 0.44\text{K}$. We find that most susceptibilities except for $\chi_{\mathbf{q}=0, \omega=0}^{K\sigma_0, K\sigma_0}$ and $\chi_{\mathbf{q}=0, \omega=0}^{+\sigma_y, -\sigma_y}$ receive a large contribution from the interband transitions and gradually increases with the ultraviolet energy cutoff [29]. We truncate to 508 bands per valley (corresponding to energy cutoff $\sim 2.5\text{eV}$) and the results are summarized in Fig.S1.

Fig. S1a) illustrates the competition between sublattice even ($\chi_{\mathbf{q}=0, \omega=0}^{K\sigma_0, K\sigma_0}$) and odd ($\chi_{\mathbf{q}=0, \omega=0}^{K\sigma_z, K\sigma_z}$) susceptibilities as a function ν . The former (at zero temperature) is equal to the Fermi surface density of states in a single valley N_F

and therefore, it depends sensitively on ν . It vanishes when the Fermi level approaches the Dirac points (which is at $\nu = -2$ in our bandstructure model) and increases rapidly as the hole densities increases. In contrast, $\chi_{\mathbf{q}=0, \omega=0}^{K\sigma_z, K\sigma_z}$ shows very weak ν dependence because the $q = 0$ susceptibility does not have any intra-band contribution when the band has a C_2T symmetry where C_2 and T are inversion and spinless time-reversal symmetry. As a result, it must be larger than N_F as $\nu \rightarrow -2$. This shows that the sublattice polarizability enhanced by a factor of $[1 - (u_0 + u_\perp)\chi_{\mathbf{q}=0, \omega=0}^{K\sigma_z, K\sigma_z}]^{-1}$ is typically stronger than the enhanced valley polarizability $N_F/[1 - (u_0 - u_\perp)N_F]$ except for filling factor close to $\nu = -3$. Recall $u_\perp > 0$.

Fig. S1b) shows the susceptibility associated with neutral excitations where the particle and hole are drawn from opposite valley. There are four layer-diagonal, sublattice dependent susceptibility denoted by $\chi^{\tau+\sigma_i, \tau-\sigma_i}$, $i = x, y, z, 0$. The mixing between different channels are not considered, a justified approximation in the limit $\mathbf{q} = \omega = 0$ due to the D_6 and spinless time reversal symmetry of twisted bilayer graphene. As an example, we demonstrate that the sublattice even and odd intervalley susceptibilities decouple: The C_3 symmetry acts as $\exp(-i\frac{2\pi}{3}\tau_z\sigma_z)$ in the valley-sublattice pseudospin space. It commutes with $\tau_\pm\sigma_{x,y}$ but rotate $\tau_\pm\sigma_{0,z}$ by a phase factor $\exp(\pm i\frac{2\pi}{3})$. Therefore, $\chi_{\mathbf{q}, \omega}^{\tau+\sigma_{0,z}, \tau-\sigma_{x,y}} = \exp(\pm i\frac{2\pi}{3})\chi_{R_{2\pi/3}\mathbf{q}, \omega}^{\tau+\sigma_{0,z}, \tau-\sigma_{x,y}}$ so it must vanish at $\mathbf{q} = 0$. Since intervalley sublattice even channels do not mix with sublattice odd ones and Fig. S1b) shows that the former have small susceptibilities, they can be neglected in the effective interaction in the main text. When the particle and hole drawn from opposite valleys are also from opposite layers, the susceptibility is significantly larger than those that are layer-diagonal as shown in Fig. S1b). The origin of the enhanced susceptibility in this channel is due to a (small-twist-angle) emergent $C_2P = \tau_x\sigma_x l_y$ symmetry in twisted bilayer graphene discovered in Ref. [36]. Because of C_2P , $\langle K, -n, \mathbf{k} | \tau_+ \sigma_x l_y | K', n, \mathbf{k} \rangle \approx 1$ where P is a unitary particle-hole symmetry [36] and $\pm n$ bands are C_2P partners. The large matrix elements between the C_2P partners result in a large $\chi^{+\sigma_x l_y, -\sigma_x l_y}$ according to Eq. S3. Note that this susceptibility dominates other pseudospin particle-hole channels when the Fermi level approached the Dirac points and might lead to an intervalley exciton condensation. The resulting valley XY-like order parameter $\tau^+\sigma_x l_y$ preserves a spinless time reversal symmetry $\mathcal{T} = \tau_y \mathcal{K} (\mathcal{T}^2 = -1)$, and hence is consistent with the previously proposed Kramers-intervalley coherent order at $\nu = -2$ [35, 36]. Note the tendency towards valley-XY order generates a strong valley-singlet repulsion via the Berk-Schrieffer diagram, as discussed in the main text. However, because this repulsion is also off-diagonal in sublattice (like Γ^{AB}) and the C_2 and C_3 symmetry decouple interaction according to their sublattice parity in the linearized gap equation (as shown in the next section), superconductivity prevails as long as intra-sublattice is attractive ($\Gamma^{AA} < 0$). In the main text and in what follows, we neglect valley-singlet repulsion generated by all the valley-XY fluctuations since the channels that modify intra-sublattice attraction is very small. In this case, suppression of valley-singlet superconductivity close to $\nu = -2$ will only require a mundane explanation – a reduced density of states.

We would also like to point out that in the definition of the susceptibility in Eq. (S2) the particle-hole momentum \mathbf{q} is, rigorously speaking, conserved only up to moiré reciprocal vectors \mathbf{G} and therefore the bare susceptibility $\chi_{\mathbf{q}, \omega}$ used in the generalized RPA formula in the main text should be understood as a matrix in the momentum space, $\hat{\chi}_{\mathbf{q}, \omega}(\mathbf{G}, \mathbf{G}')$. However, for the purpose of comparing the relative strength of susceptibilities in various channels, it is adequate to focus on the small \mathbf{q} and $\mathbf{G} = \mathbf{G}' = 0$.

II. LINEARIZED GAP EQUATION

In this section, we study the linearized gap equation within the reduced interaction model described by Eqs. (1) and (2) in the main text. The real-space interaction model is given by the Hamiltonian

$$H_{\text{red}} = \int d^2\mathbf{r} \sum_{l, l', \tau, \sigma, \sigma'} \Gamma^{\sigma\sigma'} \delta_{l, l'} \delta_{\tau, -\tau'} \psi_{l\tau\sigma}^\dagger(\mathbf{r}) \psi_{l'\tau'\sigma'}^\dagger(\mathbf{r}) \psi_{l'\tau'\sigma'}(\mathbf{r}) \psi_{l\tau\sigma}(\mathbf{r}), \quad (\text{S4})$$

where l, l' label layer, τ, τ' label valley and σ, σ' denote sublattice. The interaction matrix $\Gamma^{\sigma\sigma'} = \Gamma^{AA}\delta_{\sigma, \sigma'} + \Gamma^{AB}\delta_{\sigma, -\sigma'}$. This leads to the following linearized gap equation

$$\Delta_{\sigma\sigma'}^l(\mathbf{G}) = \Gamma^{\sigma\sigma'} \sum_{l'\sigma_1\sigma_1'} \Pi_{l\sigma\sigma', l'\sigma_1\sigma_1'}(\mathbf{G}, \mathbf{G}') \Delta_{\sigma_1\sigma_1'}^{l'}(\mathbf{G}'), \quad (\text{S5})$$

where \mathbf{G} and \mathbf{G}' are moiré reciprocal lattice vectors. The layer and sublattice-dependent pair susceptibility

$$\Pi_{l\sigma\sigma', l'\sigma_1\sigma_1'}(\mathbf{G}, \mathbf{G}') = \sum_{mm'\mathbf{k}'} \frac{n_F(\epsilon_{m\mathbf{k}'}) - n_F(-\epsilon_{m'\mathbf{k}'})}{\epsilon_{m\mathbf{k}'} + \epsilon_{m'\mathbf{k}'}} \langle m'\mathbf{k}' | e^{i\mathbf{G}\cdot\mathbf{r}} | m\mathbf{k}' \rangle_{l\sigma'\sigma} \langle m'\mathbf{k}' | e^{i\mathbf{G}'\cdot\mathbf{r}} | m\mathbf{k}' \rangle_{l'\sigma_1'\sigma_1}^*, \quad (\text{S6})$$

where m and m' are band indices. For the above contact-interaction model, the interaction matrix is independent of moiré momentum \mathbf{k} , suggesting the superconducting pairing potential exhibits moiré periodicity in the real space. The critical temperature is obtained by equating the largest eigenvalue of matrix $-\Gamma \cdot \Pi$ to 1. We numerically diagonalized this matrix as a function of the input $(\Gamma^{AA}, \Gamma^{AB})$ and this leads to the result shown in Fig. 1 of the main text. The results we obtained are not qualitatively modified by the factor $\delta_{l,l'}$ we used to simplify Eq. (S4).

For MATBG, the largest contribution to the pair susceptibility come from the flat conduction and valence bands and the Bloch wavefunctions from these bands are localized at small moiré G -vectors (i.e. they vary slowly in the moiré unit cell). Therefore, although the eigenvector of the Eq. 5 has a very large dimension, most of the properties of the superconducting order parameter can be understood in the subspace of $\mathbf{G} = \mathbf{G}' = 0$. In this subspace, the pairing amplitude of a spin-polarized valley-singlet superconductor can be conveniently described by the following 2×2 matrix,

$$F_{\sigma\sigma'}(\mathbf{k}) = \langle c_{K\sigma\uparrow}(\mathbf{k})c_{K'\sigma'\uparrow}(-\mathbf{k}) \rangle, \quad (\text{S7})$$

where we assume all electrons are from the same layer. The linearized gap equation takes a much simpler form,

$$\Delta_{\sigma\sigma'}(\mathbf{k}) = \sum_{\mathbf{k}'\sigma_1\sigma'_1} \Gamma_{\mathbf{k}\mathbf{k}'}^{\sigma\sigma'} \Pi_{\sigma\sigma',\sigma_1\sigma'_1}(\mathbf{k}') \Delta_{\sigma_1\sigma'_1}(\mathbf{k}'). \quad (\text{S8})$$

We reinserted the momentum \mathbf{k}, \mathbf{k}' dependence above for the clarity of analysis below. This sublattice dependent gap equation for MATBG in the $\mathbf{G} = \mathbf{G}' = 0$ subspace is reminiscent to the spin-dependent gap equation in ^3He . However, unlike ^3He , the sublattice pseudospin conservation is broken in MATBG by the non-interaction single-particle Hamiltonian. Because the order parameter matrix must be anti-symmetric under transposition, *i.e.* $\Delta(\mathbf{p}) = -\Delta^T(-\mathbf{p})$, where $\mathbf{p} = \mathbf{K} + \mathbf{k}$, and the parity operator \mathcal{C}_2 flips sublattice polarization $\sigma \rightarrow -\sigma$ and momentum $\mathbf{p} \rightarrow -\mathbf{p}$, we have $\mathcal{C}_2 \Delta_{\sigma,\sigma'}(\mathbf{p}) \rightarrow \Delta_{-\sigma,-\sigma'}(-\mathbf{p}) = -\Delta_{-\sigma',-\sigma}(\mathbf{p})$. Here we note that, unlike spin in ^3He , the pseudospin is flipped by the parity operator and this means the even-parity is a singlet while the odd-parity is a triplet,

$$\Delta(\mathbf{p}) = g_0(\mathbf{p})\sigma^z + (\mathbf{d}(\mathbf{p}) \cdot \boldsymbol{\sigma})\sigma^z = \begin{pmatrix} g_0 + d^z & d^+ \\ d^- & -g_0 + d^z \end{pmatrix}, \quad (\text{S9})$$

where $g_0(-\mathbf{p}) = g_0(\mathbf{p})$ and $\mathbf{d}(-\mathbf{p}) = -\mathbf{d}(\mathbf{p})$. The normal state \mathcal{C}_2 symmetry then decouples the (sublattice-pseudospin) singlet-triplet channel of the gap equation:

$$g_0(\mathbf{k}) = \sum_{\mathbf{k}'} \Gamma_{\mathbf{k}\mathbf{k}'}^{AA} \Pi^{zz}(\mathbf{k}') g_0(\mathbf{k}'), \quad (\text{S10})$$

$$\begin{pmatrix} d^z \\ d^+ \\ d^- \end{pmatrix}_{\mathbf{k}} = \sum_{\mathbf{k}'} \hat{\Gamma}_{\mathbf{k}\mathbf{k}'} \begin{pmatrix} \Pi^{00} & \Pi^{0-} & \Pi^{0-} \\ \Pi^{0-} & \Pi^{++} & \Pi^{+-} \\ \Pi^{0-} & \Pi^{+-} & \Pi^{++} \end{pmatrix}_{\mathbf{k}'} \begin{pmatrix} d^z \\ d^+ \\ d^- \end{pmatrix}_{\mathbf{k}'} \quad (\text{S11})$$

where $\hat{\Gamma}_{\mathbf{k}\mathbf{k}'} = \text{diag}\{\Gamma_{\mathbf{k}\mathbf{k}'}^{AA}, 2\Gamma_{\mathbf{k}\mathbf{k}'}^{AB}, 2\Gamma_{\mathbf{k}\mathbf{k}'}^{AB}\}$, and

$$\Pi^{ij}(\mathbf{k}) = \frac{1}{2} \sum_{\sigma\sigma',\sigma_1\sigma'_1} (\sigma^i)_{\sigma\sigma'} (\sigma^j)_{\sigma_1\sigma'_1} \Pi_{\sigma\sigma',\sigma_1\sigma'_1}(\mathbf{k}), \quad i, j = 0, z, \pm. \quad (\text{S12})$$

Since superconductivity is an instability of the Fermi surface, it is unlikely to happen in the even-parity channel (i.e. $g_0 = 0$) due to the following reasons. First, the intra-band contribution to even-parity pairing susceptibility Π^{zz} vanishes since the sublattice polarization is not established in the normal state, indicating $\langle m\mathbf{k}|\sigma^z|m\mathbf{k} \rangle = 0$ in Eq. (S6). Secondly, the inter-band contribution to Π^{zz} is negligible because the critical temperature $T_c \ll$ band separation. When $g_0 = 0$, \mathbf{d} alone cannot give rise to finite sublattice polarization, so $\langle \sigma_z \rangle = 0$ in the superconducting state and it remains nearly sublattice polarized for $T < T_c$.

In the odd-parity triplet subspace, when Γ^{AA} and Γ^{AB} are momentum independent and $\Gamma^{AB} \gg -\Gamma^{AA} > 0$, the gap equation admits a simple self-consistent solution with $d^\pm(\mathbf{k}) = 0$ and $d^z(\mathbf{k}) = d^z$ (i.e. independent of k). This parameterization simplifies the 3×3 matrix equation (Eq. (S11)) to the following equation:

$$\Gamma^{AA} \sum_{\mathbf{k}} \Pi^{00}(\mathbf{k}, T_c) = -1, \quad \Gamma^{AA} < 0. \quad (\text{S13})$$

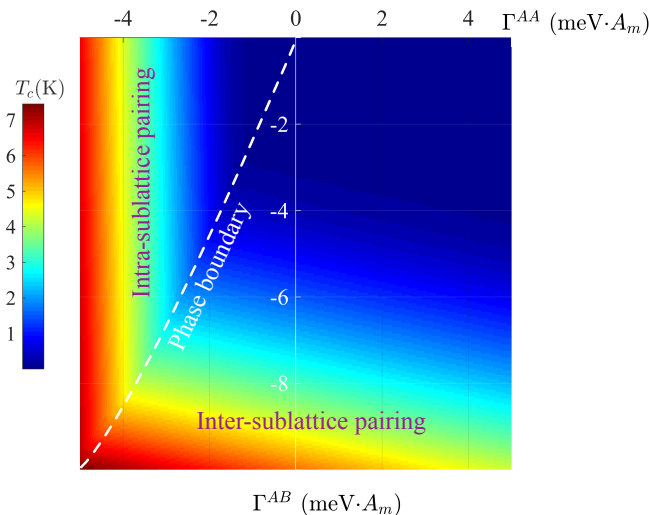


FIG. S2. Color plot of critical temperature T_c as function of Γ_{AA} and $\Gamma_{AB} \leq 0$, where A_m denotes the area of moiré supercell. The dashed curve highlights the phase boundary between the intra- and inter-sublattice pairing states. These numerical results are obtained by using a continuum model for MATBG with $t_{AA}/t_{AB} = 0.7$ and filling factor $\nu = -2.4$.

This simplification occurs because $\sum_{\mathbf{k}} \Pi^{0-}(\mathbf{k}) = 0$ which follows from C_3 rotation symmetry: $\Pi^{0-}(C_3\mathbf{k}) = e^{-4\pi i/3}\Pi^{0-}(\mathbf{k})$. Clearly, T_c obtained from this simplified gap equation is independent of Γ^{AB} . This means when the two members of the Cooper pairs are from the same sublattice, they can avoid the strong inter-sublattice repulsion Γ^{AB} if the pairing amplitude is uniform on the Fermi surface.

While we do not have compelling arguments to think that MATBG will be located in the parameter space where Γ^{AB} is attractive, it nevertheless lead to superconductivity, as shown in Fig. S2. Let us discuss the structure of the superconducting order parameter in this parameter space without dwelling with the microscopic origin of an attractive Γ^{AB} . In the parameter space where $\Gamma^{AA} \gg -\Gamma^{AB} > 0$, we can write down two degenerate self-consistent solutions $(d^z(\mathbf{k}), d^+(\mathbf{k}), d^-(\mathbf{k})) = (0, d^+, 0)$ and $(d^z(\mathbf{k}), d^+(\mathbf{k}), d^-(\mathbf{k})) = (0, 0, d^-)$ to reduce the 3×3 matrix equation to a single gap equation which is independent of Γ^{AA} :

$$\Gamma^{AB} \sum_{\mathbf{k}} \Pi^{++}(\mathbf{k}, T_c) = \Gamma^{AB} \sum_{\mathbf{k}} \Pi^{--}(\mathbf{k}, T_c) = -1, \quad \Gamma^{AB} < 0. \quad (\text{S14})$$

This is again due to the property $\sum_{\mathbf{k}} \Pi^{+-}(\mathbf{k}) = 0$ which follows from C_3 : $\Pi^{+-}(C_3\mathbf{k}) = e^{4\pi i/3}\Pi^{+-}(\mathbf{k})$. The phase boundary marked in Fig. 2 denotes the change of superconducting order parameter from intrasublattice-like $\mathbf{d}(\mathbf{k}) = d^z$ to intersublattice-like $\mathbf{d}(\mathbf{k}) = d^+$ or d^- . In this simple analysis, we can always reduce the 3×3 linearized gap equation for the C_2 triplet to a scalar equation which only involves either Γ^{AA} or Γ^{AB} . Hence, intra-sublattice Cooper pairs do not ‘see’ Γ^{AB} and the inter-sublattice Cooper pairs do not ‘see’ Γ^{AA} . When we account for non-local correction from larger moiré reciprocal vector, such perfect decoupling of Γ^{AA} and Γ^{AB} is no longer exact and T_c can indeed be suppressed by the repulsion. For reasons that are unclear to us, such suppression occurs in a very asymmetrical way. The suppression of intra-sublattice pairing ($\Gamma^{AA} < 0$) via repulsive Γ^{AB} only becomes significant when the repulsion exceeds the attraction by a factor of 10, $\Gamma^{AB} \sim -10\Gamma^{AA} > 0$. On the other hand, the suppression of inter-sublattice pairing ($\Gamma_{AB} < 0$) from repulsive Γ^{AA} is very effective – when the repulsion Γ^{AA} is roughly the same as the attraction Γ^{AB} , the T_c is already negligibly small.

III. VALLEY-TRIPLET, SPIN-SINGLET PAIRING AND BERK-SCHRIEFFER DIAGRAMS

In the maintext we assume the two members of a Cooper pair are from opposite valleys because they are related by a (spinless) time-reversal symmetry. When they are drawn from the same valley, the band-energy is usually pair breaking but it is nevertheless interesting to carry out the paramagnon analysis in this valley-triplet channel. When the superconducting order parameter is uniform, valley-triplet has to be a spin-singlet so the four external particle-lines of the particle-particle irreducible interaction Γ shown in Fig. 3a of the main text are given by 1, 2, 3, 4 =

TABLE I. A summary of important properties for the charge fluctuation and 7 pseudospin paramagnons.

T	$\tau_0\sigma_0$	$\tau_0\sigma_z$	$\tau_z\sigma_z$	$\tau_z\sigma_0$	$\tau_+\sigma_{x,y}$	$\tau_+\sigma_{0,z}$
Types of fluctuation	Charge and Pseudospin Density			Berk-Schrieffer		
Dominant scattering vertex	Direct	Exchange				
Exchange enhancement	–	$-4 < \nu < 4$		$ \nu - 2 \rightarrow 1$	$ \nu - 2 \rightarrow 0$	–
Types of Order	–	Sublattice-Polarized	Orbital-Moment	Valley-Ising	Valley-XY (IVC)	–

$K \uparrow, K \downarrow, K \downarrow, K \uparrow$. Since pairing occurs in the valley-projected Hilbert space, the diagrammatics is similar to the original Berk-Schrieffer analysis [22] with an extra sublattice degree of freedom. In particular, the pseudospin-density fluctuation contribution to A^a is

$$\begin{aligned}
A^a &= \frac{1}{2} (T^{\sigma_z s_0} - T^{\sigma_z s_z}) \\
&= \frac{1}{4} \left(\frac{-u_0}{1 - u_0 \chi^{\sigma_z s_0, \sigma_z s_0}} + \frac{u_0}{1 - u_0 \chi^{\sigma_z s_z, \sigma_z s_z}} \right) = 0.
\end{aligned} \tag{S15}$$

The last equation is due to $\chi^{\sigma_z s_z, \sigma_z s_z} = \chi^{\sigma_z s_0, \sigma_z s_0}$ and it happens because the valley-projected space is fully spin-polarized. As a result, sublattice fluctuations do not generate attractive interaction in the spin-singlet valley-triplet channel.

Let us now elaborate on the discuss of the Berk-Schrieffer (BS) transverse fluctuation contributions indicated in Fig. 3 of the main text. The particle-hole channels in the BS diagrams decouple into four channels $\tau_+\sigma_{0,x,y,z}$ in the long wavelength limit and they change

$$A^{s,a} \rightarrow A^{s,a} \mp \frac{1}{2} \sum_{i=x,y} T^{\tau+\sigma_i} - \frac{1}{2} \sum_{\delta=0,z} T^{\tau+\sigma_\delta}, \tag{S16}$$

where the intervalley intrasublattice interaction $T^{\tau+\sigma_\delta}$ is suppressed by small matrix-elements at the vertex because they mix states from opposite Chern band while the inter-valley component is given by the following:

$$T^{\tau+\sigma_i} = -\frac{u_0^2 \chi_{\mathbf{k}+\mathbf{k}',\omega}^{\tau+\sigma_i, \tau-\sigma_i}}{1 - u_0 \chi_{\mathbf{k}+\mathbf{k}',\omega}^{\tau+\sigma_i, \tau-\sigma_i}}, \quad i = x, y. \tag{S17}$$

Here the susceptibility χ is shown in Fig. 1b. While this leads to a repulsive Γ^{AB} , it does not modify Γ^{AA} hence superconductivity prevails as shown in the maintext (Fig. 1). If the interaction is mainly enhanced at zero paramagnon momentum $q = 0$, then valley-Ising paramagnon ($T^{\tau+\sigma_0}$) with $\mathbf{q} = \mathbf{k} - \mathbf{k}'$ scatters Cooper pairs locally around the Fermi surface while the valley-XY paramagnon ($T^{\tau+\sigma_{x,y}}$) with $\mathbf{q} = \mathbf{k} + \mathbf{k}'$ scatters Cooper pairs across the Fermi surface, the latter is similar to the short-range repulsive interaction generated by antiferromagnetic paramagnon in cuprates [55]. We summarize important information about different pseudospin paramagnons in Table. 1.